Available online at www.sciencedirect.com

ScienceDirect

Ceramics International 40 (2014) 2229–2235

CERAMICS INTERNATIONAL

www.elsevier.com/locate/ceramint

Multiferroic based reddish brown pigments: $Bi_{1-x}M_xFeO_3$ (M = Y and La) for coloring applications

Vineetha James, P. Prabhakar Rao*, S. Sameera, S. Divya

Materials Sciences and Technology Division, CSIR-National Institute for Interdisciplinary Science and Technology (NIIST), Thiruvananthapuram 695019, India

Received 16 July 2013; received in revised form 29 July 2013; accepted 29 July 2013
Available online 11 August 2013

Abstract

Multiferroic based reddish brown pigments: $Bi_{1-x}M_xFeO_3$ (M = Y and La) were synthesized by the conventional solid state route. The structure and morphology of the developed pigments were characterized using powder X-ray diffractometer (XRD) and scanning electron microscope (SEM) respectively. UV–vis NIR Spectrophotometer was employed to investigate the optical properties. The results indicated that the incorporation of Y^{3+} and La^{3+} offered a fine bandgap tuning contrastingly in the range from 1.95 to 2.23 eV. The color characteristics were evaluated and the typical pigment $Bi_{0.9}Y_{0.1}FeO_3$ ($L^*=37.07$, $a^*=13.83$, $b^*=9.65$) is comparable with the commercially available brown pigment (BR 300), ($L^*=34.91$, $a^*=11.38$, $b^*=9.86$) of Kawamura Chemicals Co. Ltd., Japan. A systematic enhancement of lightness (L^*), redness (a^*) and yellowness (b^*) is seen with La doping, exhibiting a bright reddish brown hue. The coloring performance of the synthesized pigments was investigated in polymer matrix for plastic coloring applications. The influence of low toxic rare earth elements as dopants on the optical properties and color performance of multiferroic $BiFeO_3$ positions them in the class of lead free inorganic red pigments for coloring applications.

Keywords: Reddish brown pigment; Bismuth iron oxide; Yttrium; Lanthanum; Color analysis

1. Introduction

One of the challenging issues in most of the inorganic pigments is the presence of toxic metals such as lead, chromium and cadmium that adversely affect the environment and human health if the quantity exceeds the critical level. The industrially available red pigments are almost exhausted by the following systems: $Al_2O_3 \cdot Cr^{3+}$(corundum), $ZnAl_2O_4 \cdot Cr$, $CaSnSiO_5 \cdot Cr^{3+}$(sphene), $MnAl_2O_4 \cdot Cr^{3+}$ (spinel), $ZrSiO_4 \cdot Fe^{3+}$(zircon), and $CdS \cdot CdSe$ (greenockite) and $Y_2Sn_{2-x}Cr_xO_{7-\delta}$ [1–3]. The cadmium based pigments give superior red shades in which toxic cadmium can enter the environment in a bioavailable form through waste-disposal sites and incineration plants [4]. This toxicity issue has led to restrictions, based on the precautionary measures that strongly limit the use of cadmium based pigments. Since there is no alternative to inorganic pigments for mass coloration of materials such as glasses, glazes and ceramic bodies, inorganic pigments which are free from toxic elements are in high demand for decorative and protective coating applications [5]. Jansen and Letschert [6] reported non toxic deep red pigments based on $CaTaO_2N$ and $LaTaON_2$. Although these pigments show an excellent hue, the starting materials are heated in a flow of toxic and inflammable ammonia gas for 20–60 h during the synthesis [6]. Praseodymium doped CeO_2 ceramic pigments developed by Bondioli et al. [7] are appealing as they produce colors ranging from brick red to dark brown [7]. The substitution of Fe_2O_3, ZrO_2, SnO_2, MnO_2, SiO_2 in CeO_2–PrO_2 have also been investigated by our research group and yielded various reddish brown hues [8–10]. At present, the search for the new red shade pigments is a high priority field, as a result of the implementation of new technologies and new environmental requirements. Recently bismuth transition metal based systems such as $BiVO_4$, Bi_2MoO_6, $BiREMoO_6$, $BiREWO_6$ have already reported to have low toxicity rating and are considered potential pigments as non-toxic alternatives [11,12]. So much attention has been devoted to the quest for non-toxic alternatives based on bismuth transition metal systems for new pigment systems with good color characteristics that may substitute for those commercially available, which in most cases do not meet the environmental requirements of the moment.

*Corresponding author. Tel.: +91 471 2515311; fax: +91 471 2491712.
E-mail address: padala_rao@yahoo.com (P. Prabhakar Rao).

0272-8842/$ - see front matter © 2013 Elsevier Ltd and Techna Group S.r.l. All rights reserved.
http://dx.doi.org/10.1016/j.ceramint.2013.07.141

Bismuth iron ($BiFeO_3$) is a well known multiferroic material having rhombohedral symmetry belonging to R3c space group. It has been a focal point of research for their technological and scientifically important applications such as photocatalytic compounds, infrared detectors, ultra-fast optoelectronic devices etc. The experimental investigations indicate that Bi undergoes easy evaporation during material preparation and generates bismuth vacancies. Moreover, it suffers severe property deteriorations due to defects and non-stoichiometry such as secondary phases, cation vacancies, oxygen vacancies, and valence fluctuation of iron ions. Recent literature reports suggest that the above defects can be overcome by partial substitution of Bi by rare-earth or alkaline-earth elements [13–17]. Kumar et al. [18] and Mukherjee et al. [19] investigated the influence of rare earth doping on the bandgap of BFO. Due to the fact that $BiFeO_3$ is a lead free structure, it opens new possibilities to give some insight into the design of inorganic pigments for coloring applications. It is fascinating to find that there is no report on its color performance. The main focus of this work is to analyze the effect of rare earth doping in $BiFeO_3$ on pigmenting properties. The compositions $Bi_{1-x}M_xFeO_3$ (M=Y, La; x=0, 0.05, 0.1, 0.15, 0.2) were synthesized by the solid state reaction method and the coloring performance was evaluated in polymer matrix for the coloring applications in plastic.

2. Experimental procedure

2.1. Sample preparation

The bismuth iron based pigments with a general formula, $Bi_{1-x}M_xFeO_3$ (M=Y, La; x=0, 0.05, 0.1, 0.15, 0.2) were synthesized by the conventional solid state route. The raw materials Bi_2O_3, Fe_2O_3 and Y_2O_3, La_2O_3 (Sigma-Aldrich, 99.99% purity) were weighed in stoichiometric ratio, homogenized by wet mixing with acetone in an agate mortar. The homogenized products were then pelletized and calcined in platinum crucibles in an electric furnace at 700 °C for 6 h. The temperature of the furnace is programmed with an initial heating rate of 10 °C/min upto 500 °C followed by a heating rate of 5 °C/min to attain 700 °C. The calcinations were repeated at 800 °C for 1–5 h with intermittent grinding to ensure the completion of reaction.

2.2. Sample characterization

The obtained powders were characterized by powder X-ray diffraction (XRD) using a Ni filtered Cu-Kα radiation (λ=1.5414 Å) with a X'pert Pro PANalytical diffractometer. Data were collected by a step scanning of 2θ from 10° to 90°. Morphological analysis of the powders was performed by a scanning electron microscope (JEOL JSM-5600LV SEM). UV–vis NIR spectra were recorded by Shimadzu, UV-3600 spectrophotometer through diffuse reflectance technique using polytetrafluoroethylene (PTFE) as a reference. The tauc plot was employed to estimate bandgap energies (Eg) of the synthesized samples from diffuse reflectance data which was used to calculate the absorption coefficient from the Kubelka–Munk [20,21] (KM) function defined as: $F(R_\infty)=\alpha/S=(1-R_\infty)^2/2R_\infty$ (Eq. 1), where $R_\infty=R_{sample}/R_{PTFE}$. Here α is the absorption coefficient, S is the scattering coefficient, and $F(R_\infty)$ is the KM function. The energy dependence of semiconductors near the absorption edge is expressed as: $\alpha h\nu=K(E-Eg)^\eta$ (Eq. 2). Here E is the incident photon energy ($h\nu$), Eg is the optical absorption edge energy, K is a constant, and the exponent η is dependent on the type of optical transition as a result of photon absorption [22]. The band gap can be evaluated using tauc plot by extrapolating the linear portion of $(F(R_\infty)h\nu)^2$ versus ($h\nu$) and the intercept of the line on the abscissa ($F(R_\infty)h\nu)=0$) gives the value of optical absorption edge energy. The color parameters of the pigments were determined by coupling analytical software UVPC color analysis, to the UV-3600 spectrophotometer by which the measurement conditions were kept as an illuminant D65, 10° complementary observer and measuring geometry d/8°. The CIE 1976 $L^*a^*b^*$ colorimetric method was used, as recommended by the Commission Internationale del'Eclairage (CIE). In this system, L^* is the color lightness (0 for black, 100 for white), a^* is the green (−)/red (+) axis, and b^* is the blue (−)/yellow (+) [23]. The chroma is defined as $C^*=[(a^*)^2+(b^*)^2]^{1/2}$. The hue angle, h° is expressed in degrees and ranges from 0° to 360° and is calculated using the formula $h^\circ=\tan^{-1}(b^*/a^*)$.

2.3. Coloration of plastics

To evaluate the red hue consistency of the synthesized pigment for the real application in the coloration of plastics, two samples typically $Bi_{0.9}Y_{0.1}FeO_3$ and $Bi_{0.8}La_{0.2}FeO_3$ that exhibit better chromatic properties were selected. Poly(methyl methacrylate) (PMMA) was used as the polymer matrix for making the pigmented compact. PMMA is a known water soluble polymeric material extensively used for cold extrusion of many inorganic oxides such as alumina and zirconia. A viscous solution of PMMA (90 wt%) was made using a conventional electrical coil heater and 10 wt% of the pigment was slowly added with stirring and converted to a thick paste. The paste was then transferred in a mold and compressed into cylindrical discs.

3. Results and discussion

3.1. Powder X-ray diffraction analysis

Figs. 1 and 2 present the powder XRD patterns of the samples, $Bi_{1-x}M_xFeO_3$ (M=Y, La; x=0, 0.05, 0.1, 0.15, 0.2) with different concentrations of yttrium and lanthanum. The sharp and intense peaks indicate the crystalline nature of the samples. In reference to JCPDS no.01-074-6717, it was found that all the major peaks can be indexed to rhombohedral $BiFeO_3$ with a space group R3c. XRD results indicate that the phase stability was achieved with 10 mol% yttrium doping and a trace impurity phase $Y_3Fe_5O_{12}$ is detected with further doping which can be interpreted that 10% is the solid solubility

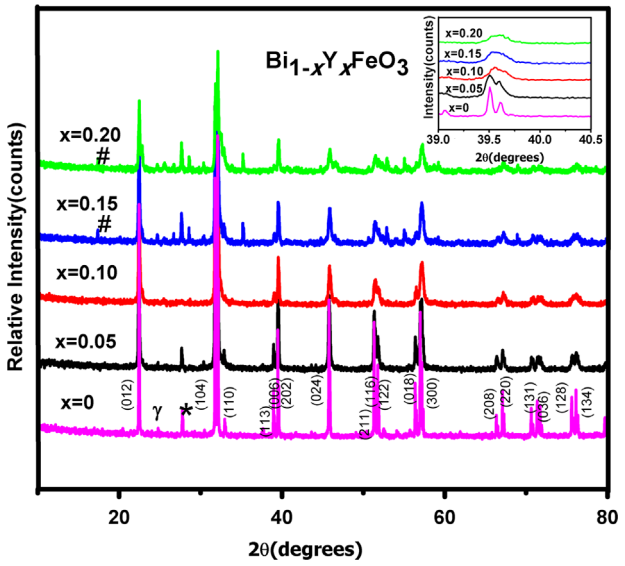

Fig. 1. Powder X-ray diffraction patterns of $Bi_{1-x}Y_xFeO_3$ (x=0, 0.05, 0.1, 0.15, 0.2) compounds. (*, $^{\gamma}$ and $^{\#}$ indicate $Bi_{25}Fe_2O_{40}$, $Bi_2Fe_4O_9$ and $Y_3Fe_5O_{12}$ phases respectively). All the diffraction peaks could be attributed to rhombohedral $BiFeO_3$ with space group R3c and 10 mol% is the solid solubility limit for yttrium doping into $BiFeO_3$ structure.

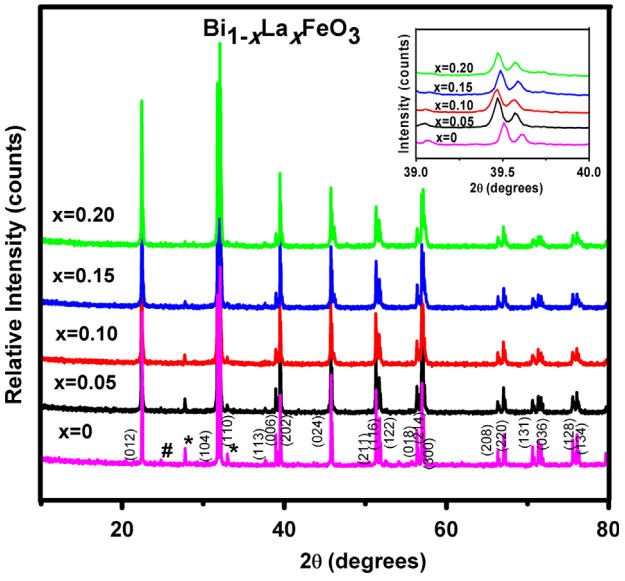

Fig. 2. Powder X-ray diffraction patterns of $Bi_{1-x}La_xFeO_3$ (x=0, 0.05, 0.1, 0.15, 0.2) compounds. (* and $^{\#}$ indicate $Bi_{25}Fe_2O_{40}$, $Bi_2Fe_4O_9$ phases respectively). All the diffraction peaks could be attributed to rhombohedral $BiFeO_3$ with space group R3c and the phase stability is achieved with 20 mol% La doping.

limit of yttrium into $BiFeO_3$ structure. The inset figure (Fig. 1) shows that, the intensity of diffraction peak (202) becomes weak with increasing Y doping and a gradual shift was observed towards higher angle as the ionic radii of Y^{3+} (90.0 pm) is smaller than Bi^{3+}(103 pm). The secondary phases, $Bi_{25}Fe_2O_{40}$ and $Bi_2Fe_4O_9$ were reported to form during the synthesis of BFO and could not be removed even by longer calcination times which could also lead to more volatilization of Bi_2O_3 [24,25]. It is observed that the 28° impurity peak is weakened with increasing doping concentration of lanthanum and no secondary phases were detected at x=0.20 indicating that the addition of La can suppress the volatilization of Bi, which otherwise leads to the existence of the 28° peak during the preparation of the solid solution [25,26]. The doping of La hardly affects the position of the peaks, which indicates that the lattice constant of the perovskite crystal remains largely unchanged, as the difference between the ionic radii of La^{3+} (103.2 pm) and Bi^{3+}(103 pm) is trivial. The average crystallite sizes (d) of the synthesized samples were calculated using Scherrer's formula, $d=K\lambda/\beta\cos\theta$ where K is dimensionless shape factor, λ is the X-ray wavelength, β is the line broadening at half the maximum intensity (FWHM), θ is the Bragg angle and are listed in Table 1. It was found that for $Bi_{1-x}La_xFeO_3$, the average crystallite size was in the range 117–140 nm which is larger than yttrium doped compounds.

3.2. Morphology

Figs. 3 and 4 show the SEM microstructure of yttrium and lanthanum doped $BiFeO_3$ samples for different doping concentrations. It is seen that the particles are bigger in size for La doped $BiFeO_3$ compared to Y substituted one and shows decreasing trend in particle size with substitution. The micrographs show highly agglomerated particles in the size range 1–5 μm.

3.3. UV–vis NIR diffuse reflectance analysis

The optical properties of the samples were studied by measuring their UV–vis NIR diffuse reflectance spectra. Figs. 5 and 6 present UV–vis NIR reflectance spectra of the prepared samples. The broad absorption band from 450 to 600 nm confirmed the absorption of higher percentage of visible light. This absorption is due to two types of electronic transitions. The first excitation is due to the electronic transition from $^6A_1$ state to $^4T_1$ (^4G) state and the second one is due to the excitation from $^6A_1$ to ^4E, $^4A_1$ (^4G) ligand field transitions and the field transfer band tail [27].These transitions overlap with each other and give a broad band as seen in Fig. 7 for La doped samples and the similar spectra is observed with Y doping also. The band around 680 nm is due to metal-to-metal transition, and the one around 850 nm is due

Table 1
Crystallite size of $Bi_{1-x}M_xFeO_3$ (M=Y, La; x=0, 0.05, 0.1, 0.15, 0.2). Smaller crystallite sizes for yttrium doping whereas larger crystallite sizes for La doping are observed.

Doping content (x)	Crystallite size (nm)	
	$Bi_{1-x}Y_xFeO_3$	**$Bi_{1-x}La_xFeO_3$**
0.05	84	140
0.10	57	117
0.15	62	113
0.20	111	127

to crystal field transition. The absorption below 450 nm is associated with charge transfer transition (d–d) of Fe^{3+} ions from $^6A_1$ to ^4E (^4D) and $^4T_2$ (^4D) level [28]. The rare earth doping in bismuth iron shows absorption in the wavelength region below 600 nm and thereby producing a red color. An enhancement of NIR reflectance was observed in yttrium and lanthanum doped compounds. Pure $BiFeO_3$ possesses 17% reflectance at 1100 nm from which it is enhanced to 39% and 43% by yttrium and lanthanum doping respectively.

Generally the optical absorption performance of semiconductors is related to the electronic structure feature and their bandgaps. The energy dependence of the material in the

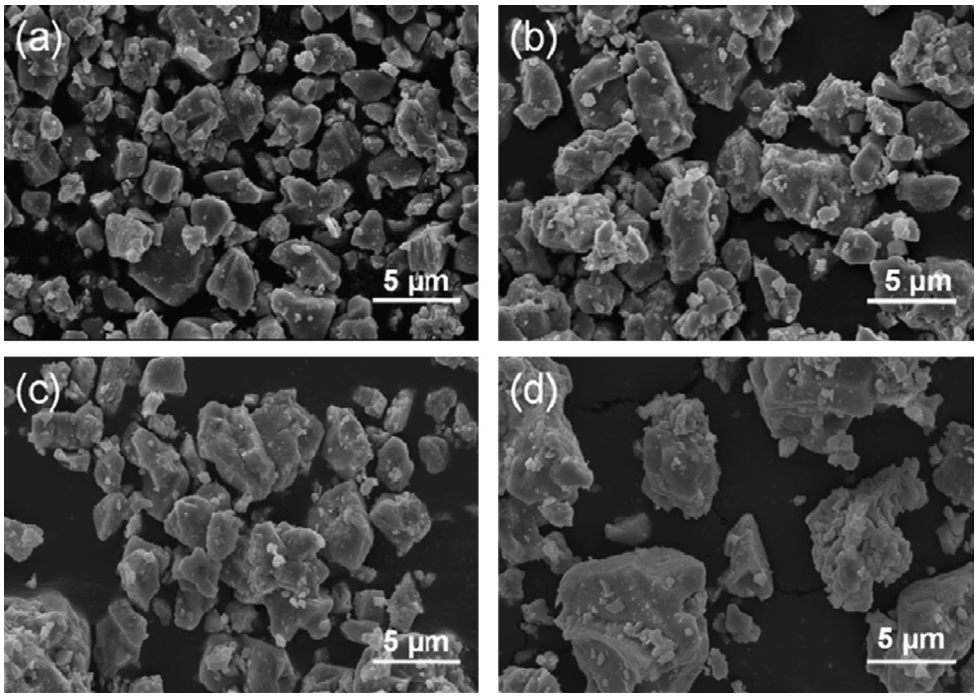

Fig. 3. SEM micrographs of $Bi_{1-x}Y_xFeO_3$ (YBFO) for (a) $x=0.05$, (b) $x=0.10$, (c) $x=0.15$, and (d) $x=0.20$. Grains are seen to be larger in size and agglomerated with increasing yttrium doping.

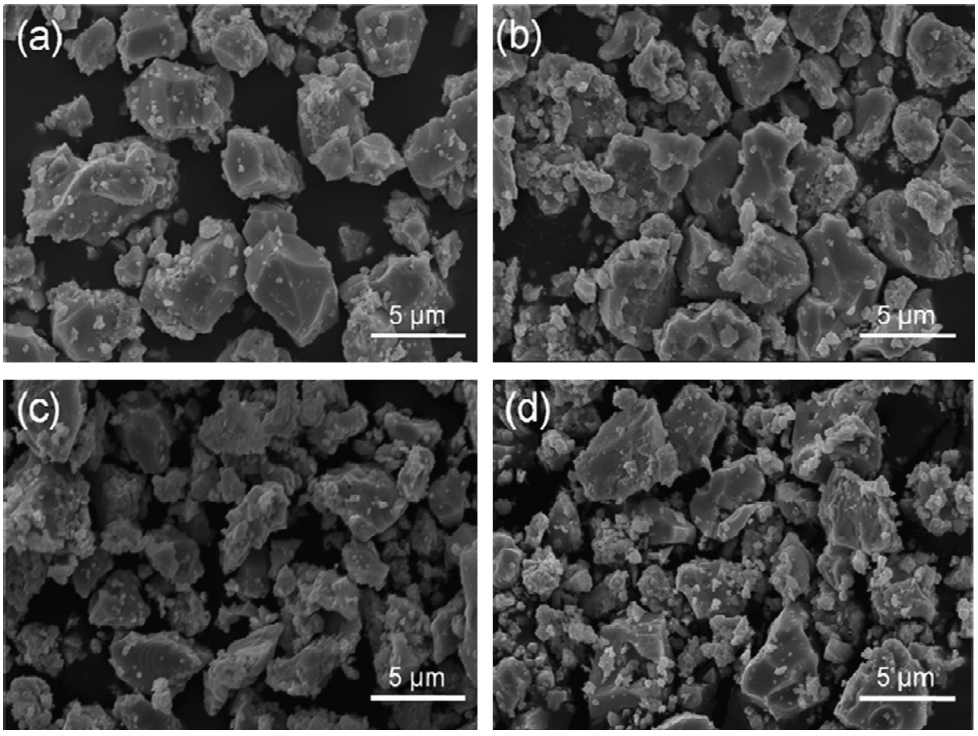

Fig. 4. SEM micrographs of $Bi_{1-x}La_xFeO_3$ (LBFO) for (a) $x=0.05$, (b) $x=0.10$, (c) $x=0.15$, and (d) $x=0.20$. Decreasing trend in grain size is seen with La doping.

UV–vis NIR was further explored. The exponent η in Eq. 2 is assigned a value of 1/2, 3/2, 2, and 3 for direct allowed, direct forbidden, indirect allowed, and indirect forbidden transitions respectively [29]. For the diffused reflectance spectra, the KM function can be used instead of α for the estimation of the optical absorption edge energy [22]. The corresponding values of direct band gap of BFO can be evaluated by extrapolating the linear portion of $(F(R_\infty)h\nu)^2$ versus $(h\nu)$. The intercept of the line on the abscissa $(F(R_\infty)h\nu)=0)$ gives the value of optical absorption edge energy. The observed bandgap value for $BiFeO_3$ is consistent with literature reports [30].The variation of bandgap with increasing yttrium and lanthanum doping is tabulated in Table 2. This contrasting variation of bandgap with increasing doping concentration might be attributed to the Burstein Moss shift caused by electrons generated by oxygen vacancy [31] arising from Bi volatility and the transition from Fe^{3+} to Fe^{2+}. Zhang et. al [26] reported the reduction of oxygen vacancies and Fe^{2+} by lanthanum doping along with a decreasing trend in bandgap [18]. Mukherjee et. al reported a contrasting trend in bandgap by yttrium doping with increasing oxygen vacancies [19]. The present results are in confirmative with the above investigations.

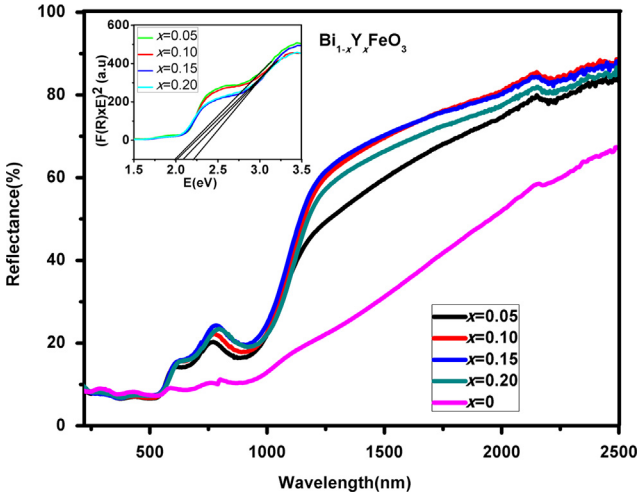

Fig. 5. Diffuse reflectance spectra of $Bi_{1-x}Y_xFeO_3$ ($x=0$, 0.05, 0.1, 0.15, 0.2). (Inset): Plot of $(F(R_\infty)h\nu)^2$ versus $(h\nu)$ for the estimation of optical bandgap. Doping of yttrium for Bi^{3+}in $BiFeO_3$ resulted in blue shifting the absorption edge to higher energy side.

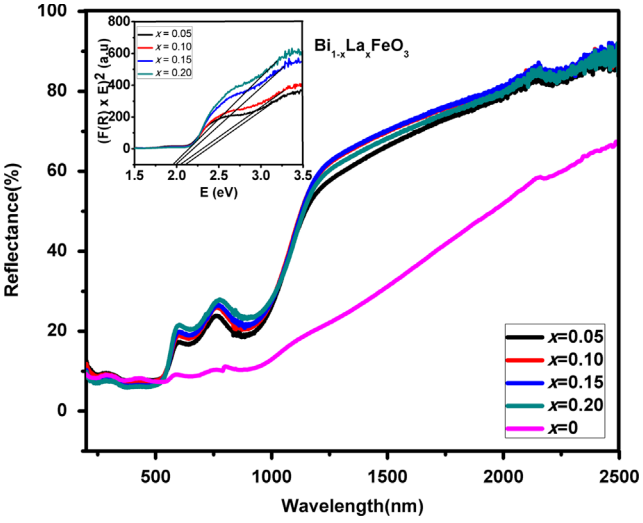

Fig. 6. Diffuse reflectance spectra of $Bi_{1-x}La_xFeO_3$ ($x=0$, 0.05, 0.1, 0.15, 0.2). (Inset): Plot of $(F(R_\infty)h\nu)^2$ versus $(h\nu)$ for the estimation of optical bandgap. Substitution of lanthanum for Bi^{3+} in $BiFeO_3$ resulted in red shifting the absorption edge to lower energy side.

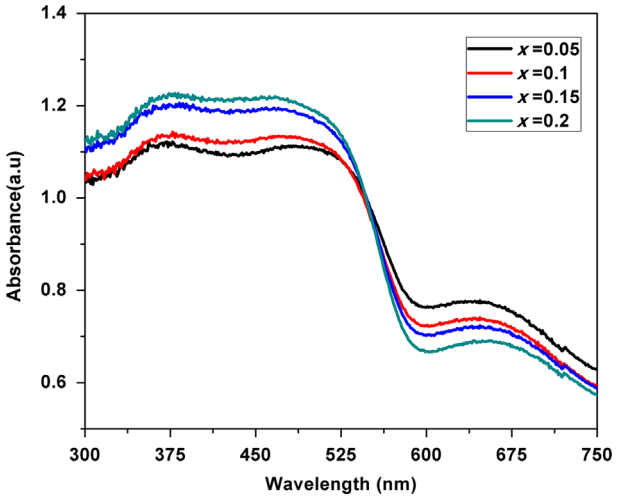

Fig. 7. Absorbance Spectra of $Bi_{1-x}La_xFeO_3$($x=0$, 0.05, 0.1, 0.15, 0.2).

3.4. Color performance

The chromatic properties of the synthesized pigments can be accessed from their CIE 1976 color coordinate values depicted in Table 2. The doping of yttrium (upto 10 mol%) results in an increase in the red component (a^*) to 13.83 and yellow component (b^*) to 9.65. A further increase in dopant concentration (up to 20 mol%) brings about a slight decrease in the red and yellow hues, as denoted by the chromatic coordinates a^* and b^*. This may be due to the appearance of $Y_3Fe_5O_{12}$ impurities seen after 10 mol% yttrium doping. Consequently the color changes to dark-brown. The color coordinates of the typical pigment $Bi_{0.9}Y_{0.1}FeO_3$ ($L^*=37.07$, $a^*=13.83$, $b^*=9.65$) are found to be higher than that of the commercially available brown pigment (BR 300), ($L^*=34.91$, $a^*=11.38$, $b^*=9.86$) of Kawamura Chemicals Co. Ltd., Japan. The doping of lanthanum results in a systematic increase in a^* and b^* values from 12.6 to 17.96 and 12.34 to 22.13 respectively, which indicates that the redness of the pigment sample enhances. The a^* and b^* values are almost same up to 10 mol% La, exhibiting bright reddish brown hue. The hue angle values reveal that the Y^{3+} and La^{3+} doped $BiFeO_3$ pigments lie in the reddish brown region of the cylindrical color space ($h^\circ=0$–35 for red and 35–70 for orange) and the photographs of the synthesized pigments are shown in Fig. 8. The significance of the results is that, chemical manipulations based on rare earth dopants such as Y and La doping offer a scope for color performance studies

Table 2
Color coordinates and band gap values of $Bi_{1-x}M_xFeO_3$ (M=Y, La; x=0, 0.05, 0.1, 0.15, 0.2).

Parameters	$Bi_{1-x}Y_xFeO_3$ (YBFO)				$Bi_{1-x}La_xFeO_3$ (LBFO)			
	$x=0.05$	$x=0.10$	$x=0.15$	$x=0.20$	$x=0.05$	$x=0.10$	$x=0.15$	$x=0.20$
L^*	36.74	37.07	35.2	34.79	40.82	41.76	41.66	42.35
a^*	12.65	13.83	12.2	12.36	12.6	14.26	16.09	17.96
b^*	9.39	9.65	7.89	7.52	12.34	15.7	19.38	22.13
C	15.76	16.6	14.53	14.47	17.63	21.21	25.19	28.5
h^o	36.59	34.91	32.87	31.31	44.39	47.76	50.31	50.93
Bandgap (eV)	1.99	2.03	2.23	2.10	2.11	2.05	1.99	1.95

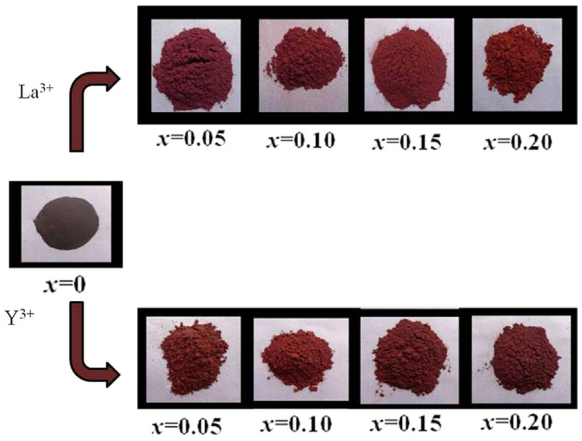

Fig. 8. Representative pictures of the synthesized pigments; $Bi_{1-x}M_xFeO_3$ (x=0, 0.05, 0.1, 0.15, 0.2; M=Y, La) compounds. Y doping gives brown color and La doping produces bright reddish brown hue. (For interpretation of the references to color in this figure legend, the reader is referred to the web version of this article.)

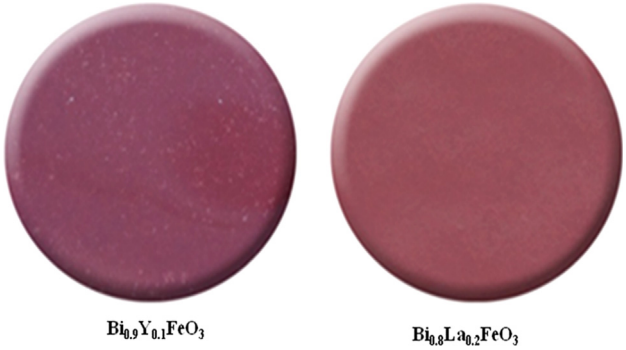

Fig. 9. Photographs of $Bi_{0.9}Y_{0.1}FeO_3$+PMMA and $Bi_{0.8}La_{0.2}FeO_3$+PMMA (10 wt%). The test pieces exhibit uniform distribution of pigment particles in the polymer matrix. (For interpretation of the references to color in this figure legend, the reader is referred to the web version of this article.)

placing them in the class of lead free inorganic pigments for coloring applications.

3.5. Coloration of plastics

The coloring performance of the typically synthesized pigments was tested for its coloring application in a substrate material like PMMA. Typically, 10 wt% pigment sample was dispersed in PMMA and compressed to a cylindrical disk (Fig. 9). The intensity of the color of plastics will depend on the concentration of the pigment. The color co-ordinates of the test pieces were measured at different locations. The $L^*a^*b^*$ values obtained were more or less the same indicating the uniform distribution of the pigment particles in the polymer matrix. Thus, the developed pigments may find potential application in the coloring of various plastic materials.

4. Conclusions

Multiferroic based reddish brown pigments: $Bi_{1-x}M_xFeO_3$ (M=Y, La) have been synthesized by solid state reaction method to analyze the limit of solid solution, stability and pigmenting properties by rare earth doping. The XRD patterns showed that small rare earth doping stabilizes the rhombohedral perovskite structure of $BiFeO_3$. The typical pigment $Bi_{0.9}Y_{0.1}FeO_3$ (L^*=37.07, a^*=13.83, b^*=9.65) is comparable to the commercially available brown pigment (BR 300), (L^*=34.91, a^*=11.38, b^*=9.86) of Kawamura Chemicals Co. Ltd., Japan. A maximum a^* of 17.96 and b^* of 22.13 was achieved with La doping giving scope for coloring applications. The powder pigmenting properties were also tested in polymer matrix for the coloration of plastics. The results imply the potential role of yttrium and lanthanum as a dopant in improving the optical properties and coloring performance of multiferroic $BiFeO_3$ which keeps them in the class of lead free inorganic pigments.

Acknowledgment

The authors acknowledge the Defense Research and Development Organization (DRDO), Govt. of India, New Delhi, India for the financial support of this work.

References

[1] G. Emiliani, F. Corbara, TecnologiaCeramica: Le Materie Prime (Ceramic Technology: Raw Materials), Grupo Editoriale Faenza Editrice S.P.A. (Italia), Faenza, Italy162–163.
[2] R. Eppler, D. Eppler, Which Colors Can and Cannot Be Produced in Ceramic Glazes, Ceramic Engineering and Science Proceedings 15 (1) (1994) 281–288.
[3] R. Stefanov, J.B. Carda Castello, V.B. Marza, J.M. Hohembergerger, New red shade ceramic pigments based on $Y_2Sn_{2-x}Cr_xO_{7-\delta}$ pyrochlore

solid solutions, Journal of the American Ceramic Society 85 (2002) 1197–1202.
[4] D. Knorn, Cadmiumemissionenbei der Verbrennung und Ablagerung von HausmuÈ ll, Metall 37 (1983) 633–635.
[5] G. Buxbaum, Industrial Inorganic Pigments, 2nd ed., Wiley-Vch, Weinheim, Germany, 1997.
[6] M. Jansen, H.P. Letschert, Inorganic yellow–red pigments without toxic metals, Nature 404 (2000) 980–982.
[7] F. Bondioli, A.M. Ferrari, L. Lusvarghi, T. Manfredini, S. Nannerone, L. Pasquali, G. Selvaggi, Synthesis and characterization of praseodymium doped ceria powders by a microwave-assisted hydrothermal route, Journal of Materials Chemistry 15 (2005) 1061–1066.
[8] L.S. Kumari, P. Prabhakar Rao, M.L.P. Reddy, Environment-friendly red pigments from CeO_2–Fe_2O_3–Pr_6O_{11} solid solutions, Journal of Alloys and Compounds 461 (2008) 509–515.
[9] L.S. Kumari, P.Prabhakar Rao, Peter Koshy, Red pigments based on CeO_2–MO_2–Pr_6O_{11} (M=Zr and Sn): solid solutions for the coloration of plastics, Journal of the American Ceramic Society 93 (5) (2010) 1402–1408.
[10] L.S. Kumari, P. Prabhakar Rao, S. Sameera, Peter Koshy, Synthesis and optical properties of $Ce_{0.95}Pr_{0.05-x}M_xO_2$ (M=Mn, Si) as potential ecological red pigments for coloration of plastics, Ceramics International 38 (2012) 4009–4016.
[11] L.S. Kumari, T.H. Gayathri, S.F. Sameera, P.Prabhakar Rao, Y-doped Bi_2MoO_6 yellow pigments for the coloration of plastics, Journal of the American Ceramic Society 94 (2011) 320–323.
[12] N. Santha, P. Koshy, M.T. Sebastian, R. Ratheesh, Preparation and characterization of bismuth rare earth tungstate ($BiREWO_6$) dielectric ceramics, Journal of Materials Science: Materials in Electronics 13 (4) (2002) 229–233.
[13] J. Dho, X. Qi, H. Kim, J.L. MacManus-Driscoll, M.G. Blamire, Large electric polarization and exchange bias in multiferroic $BiFeO_3$, Advanced Materials 18 (2006) 1445–1448.
[14] J. Liu, L. Fang, F.G. Zheng, S. Ju, M.R Shen, Enhancement of magnetization in Eu doped $BiFeO_3$ nanoparticles, Applied Physics Letters 95 (2009) 022511–022513.
[15] J.B. Li, G.H Rao, Y.G. Xiao, J. Luo, G.Y Liu, J.R Chen, J.K. Liang, Structure, dielectric and magnetodielectric properties of $Bi_{1-x}Gd_xFeO_3$ ceramics, Chinese Physics B 19 (2010) 107505–107511.
[16] Y. Du, Z.X Cheng, M. Shahbazi, E.W. Collings, S.X. Dou, X.L. Wang, Enhancement of ferromagnetic and dielectric properties in lanthanum doped $BiFeO_3$ by hydrothermal synthesis, Journal of Alloys and Compounds 490 (2010) 637–641.
[17] P. Thakuria, P.A. Joy, High room temperature ferromagnetic moment of Ho substituted nanocrystalline $BiFeO_3$, Applied Physics Letters 97 (2010) 162504–162507.
[18] N. Kumar, A. Kaushal, C. Bhardwaj, D. Kaur, Effect of La doping on structural, optical and magnetic properties of $BiFeO_3$ thin films deposited by pulsed laser deposition technique, Opto Electronics and Advanced Materials-Rapid Communications 4 (10) (2010) 1497–1502.
[19] A. Mukherjee, S.M. Hossain, M. Pal, S. Basu, Effect of Y-doping on optical properties of multiferroics $BiFeO_3$ nanoparticles, Applied Nanoscience 2 (2012) 305–310.
[20] P. Kubelka, F. Munk, Ein Beitragzur Optik der Farbanstriche, Zeitschrift fuer Technische Physik 12 (1931) 593–601.
[21] G. Kortum, Reflectance Spectroscopy Principles, Methods, Applications, Springer, New York, 1969.
[22] D.G Barton, M. Shtein, R.D. Wilson, S.L. Soled, E.J Iglesia, Structure and electronic properties of solid acids based on tungsten oxide nanostructures, Journal of Physical Chemistry B 103 (1999) 630–640.
[23] R.M. Johnston, in: T.C. Putton (Ed.), Pigment Handbook, 3, Wiley-Interscience Publication, New York, 1973, pp. 229–288.
[24] Z. Chen, J. Hu, Z Lu, X. He, Low-temperature preparation of lanthanum-doped $BiFeO_3$ Crystallites by a sol–gel-hydrothermal method, Ceramics International 37 (2011) 2359–2364.
[25] S. Kazhugasalamoorthy, P. Jegatheesan, R. Mohandoss, N.V Giridharan, B. Karthikeyan, R. Justin Joseyphus, S. Dhanuskodi, Investigations on the properties of pure and rare earth modified bismuth ferrite ceramics, Journal of Alloys and Compounds 493 (2010) 569–572.
[26] Ziang Zhang, Haiyang Liu, Yuanhua Lin, Yan Wei, Ce-Wen Nan, Xuliang Deng, Influence of La doping on magnetic and optical properties of bismuth ferrite nanofibers, Journal of Nanomaterials 238605 (2012) 610–614.
[27] Adhish Jaiswal, Raja Das, K. Vivekanand, Priya Mary Abraham, Suguna Adyanthaya, Pankaj Poddar, Effect of reduced particle size on the magnetic properties of chemically synthesized $BiFeO_3$ nanocrystals, Journal of Physical Chemistry C 114 (2010) 2108–2115.
[28] Y.P. He, Y.M. Miao, C.R. Li, S.Q. Wang, L. Cao, S.S. Xie, G.Z Yang, B.S. Zou, C. Burda, Size and structure effect on optical transitions of iron oxide nanocrystals, Physical Review B 71 (2005) 125411–125419.
[29] J. Tauc, R. Grigorov, A. Vancu, Optical properties and electronic structure of amorphous germanium, Physica Status Solidi 15 (1966) 627–637.
[30] F. Gao, X. Chen, K. Yin, S. Dong, Z. Ren, F. Yuan, T. Yu, Z. Zou, J.M. Liu, Visible-light photocatalytic properties of weak magnetic $BiFeO_3$ nanoparticles, Journal of Advanced Materials 19 (2007) 2889–2892.
[31] S.C. Roy, G.L. Sharma, M.C. Bhatnagar, Large blue shift in the optical band-gap of sol–gel derived $Ba_{0.5}Sr_{0.5}TiO_3$ thin films, Solid State Communications 141 (5) (2007) 243–247.